Quantifying an underestimated deciduous-needleleaf carbon sink at the southern margin of the central-Siberian permafrost zone

Jialin Liu [1,2,3,¶], Fangyan Cheng [4,¶], Róisín Commane [5], Yi Zhu [1,4], Weiwen Ji [6], Xiuling Man [7], ChengHe Guan [2,8*], and J William Munger [3,*]

[1] Key Laboratory of National Forestry and Grassland Administration on Ecological Landscaping of Challenging Urban Sites, Shanghai Academy of Landscape Architecture Science and Planning, Shanghai 200232, China.

[2] New York University Shanghai, Shanghai 200122, China.

[3] Harvard China Project and Department of Earth and Planetary Sciences, John A. Paulson School of Engineering and Applied Sciences, Harvard University, Cambridge 02138, United States.

[4] Coastal Ecosystems Research Station of the Yangtze River Estuary, Ministry of Education, Key Laboratory for Biodiversity Science and Ecological Engineering, Institute of Biodiversity Science, School of Life Sciences, Fudan University, Shanghai 200438, China.

[5] Department of Earth and Environmental Sciences and Lamont-Doherty Earth Observatory, Columbia University, Palisades 10964, United States.

[6] Beijing Meteorological Service Center, Beijing 100089, China.

[7] School of Forestry, Northeastern Forestry University, Harbin 150040, China.

[8] PEAK Urban Programme, the Centre of Migration, Policy and Society, University of Oxford, Oxford, OX2 6QS, United Kingdom.

*Corresponding authors: J. William Munger (jwmunger@seas.harvard.edu); ChengHe Guan (chenghe.guan@nyu.edu)

¶These authors contributed equally to this work.

Key Points:

1. Seasonality in permafrost active layer and environmental temperature-humidity dynamics closely regulate boreal larch' carbon cycle.
2. Ecosystem functional traits in deciduous larch are distinct from other boreal needleleaf evergreens.
3. By inadequately accounting for boreal larch's carbon sink, the estimates of global forest carbon budgets will bias low.

Quantifying an underestimated deciduous-needleleaf carbon sinks at the southern margin of the Central-Siberian permafrost zone

Abstract

With over 700 million km^2 Siberia is the largest expanse of the northern boreal forest—deciduous-needleleaf larch. Temperatures are increasing across this region, but the consequences to carbon balances are not well understood for larch

forests. We present flux measurements from a larch forest near the southern edge of Central-Siberia where permafrost degradation and ecosystem shifting are already observed. Results indicate net carbon exchanges are influenced by the seasonality of permafrost active layers, temperature and humidity, and soil water availability. During periods when surface soils are fully thawed, larch forest is a significant carbon sink. During the spring-thaw and fall-freeze transition, there is a weak signal of carbon uptake at mid-day. Net carbon exchanges are near-zero when the soil is fully frozen from the surface down to the permafrost. We fit an empirical ecosystem functional model to quantify the dependence of larch-forest carbon balance on climatic drivers. The model provides a basis for ecosystem carbon budgets over time and space. Larch differs from boreal evergreens by having higher maximum productivity and lower respiration, leading to an increased carbon sink. Comparison to previous measurements from another northern larch site suggests climate change will result in an increased forest carbon sink if the southern larch subtype replaces the northern subtype. Observations of carbon fluxes in Siberian larch are still too sparse to adequately determine age dependence, inter-annual variability, and spatial heterogeneity though they suggest that boreal larch accounts for a larger fraction of global carbon uptake than has been previously recognized.

Keywords Central Siberia; Boreal forests; Deciduous larch; Carbon budgets; Ecosystem functional traits

Plain language summary

Cold, wet soils in boreal forests contain a large amount of carbon. However, warmer temperatures coupled with changes in hydrology could release stored carbon and accelerate its decomposition. The boreal spruce and pine forests in North America and Fennoscandia have been studied extensively, but observations in the Siberian larch forests are limited. Because larch shed their needles in winter their response to changing temperature and moisture may differ from expectations based on evergreen conifers. Our work focuses on a larch forest in northern China that is at the southern edge of the Central-Siberian biome where eco-environmental changes are starting to occur. By studying how the annual growth and carbon balance in this forest respond to variations in weather we will be better able to predict significant changes in the structure and function of the larch ecosystem that could undermine regional ecosystem stability. Larch forest function differently from evergreen needle-leaf forests and provide a larger carbon sink than had been previously recognized.

1. Introduction

Boreal forests, the last of the wild (Watson *et al* 2018), encompass 33% of the global forest area (Brandt *et al* 2013) and account for 20% of the annual global forest carbon sink (Pan *et al* 2011). The Boreal zone spans North America, Fennoscandia, and Siberia. Siberia is the dominant region both by area and total biomass (Gauthier *et al* 2015). Circumpolar boreal forests are dominated by conifer genera (Gower *et al* 2001), notably including *Picea spp.* (spruces),

Pinus spp. (pines), and *Larix spp.* (larches). Siberian boreal larches of Eurasia are distinct from other boreal conifers due to their deciduous habit (Gower and Richards 1990, Goldammer and Furyaev 1996, Chen *et al* 2016). Several major field campaigns (e.g., ABLE-3B, BOREAS, Fluxnet-Canada, ABoVE in Canada and Alaska, and SMEAR in Finland) have generated over 70 site-years of data on boreal spruces (Bakwin *et al* 1994, Fan *et al* 1995, Pattey *et al* 1997, Gower *et al* 1997, Milyukova *et al* 2002, Bergeron *et al* 2007, Dunn *et al* 2007, Kurbatova *et al* 2008, Sulla-Menashe *et al* 2018) and over 60 site years for boreal pines (Kolari *et al* 2004, Thum *et al* 2008, Ikonen *et al* 2016, Mäki *et al* 2019). However, no more than 10 site years of data have been reported for Siberian larch (Nakai *et al* 2008, Shuman *et al* 2011, Zhang *et al* 2011, Ohta *et al* 2014, Takata *et al* 2017).

Siberia includes 700 million km^2 boreal-arctic ecosystems (Abaimov 2010). Some field experiments had been conducted for exploring ecosystem carbon budget and its micrometeorological responses in the central and east Siberian larch forests (e.g., Hollinger *et al* 1998, Nakai *et al* 2008, Dolman *et al* 2004, Matsumoto *et al* 2008, Ichii *et al* 2017, Nolan *et al* 2018). However, the available data are too limited to adequately assess vegetation functional traits for this vast, heterogeneous region (Villarreal *et al* 2018, Miles and Esau 2016). There is a critical gap in carbon budget observations for larch forests growing at the margins of the Siberian ecosystem (Pan *et al* 2011). Nolan *et al* (2018) find forests at the southern Siberian ecotone are responding markedly to climate change. Boreal ecosystems' exposure to disturbances, such as wildfires, plant diseases, insect pests, ec osystem shifting, and permafrost degradation, strongly affect their structures and functions (Sala *et al* 2000, Esper and Schweingruber 2004, Bonan 2008, Schuur *et al* 2009, Tchebakova *et al* 2009, Shuman *et al* 2011, Gauthier *et al* 2015). Likewise, cooler-tolerant forests are invaded by warmer-adapted forests migrating northward at the northern ecotone (Zhang *et al* 2011). Warming Siberian ecosystems will, in turn, accelerate the regional to global climate change through landscape albedo alteration (Bonan *et al* 1992) and release of frozen carbon (Schuur *et al* 2009, Helbig *et al* 2017). A recent study elucidated that amplified vegetation productivity may enhance the seasonal ecosystem carbon exchange in the northern ecosystem (Forkel *et al* 2016). However, without adequate representation of the full range of boreal ecosystems, especially boreal larch already experiencing climate warming, the prediction has large uncertainties.

Making eddy-covariance observations across the entire Siberia would be impractical. Ecosystem functional models are an approach to apply and test understanding based on site-specific relationships to larger regions using remotely sensed observations to account for spatial and temporal patterns (Commane *et al* 2017). The model we present is a circum-polar version of the Vegetation Photosynthesis and Respiration Model (PVPRM) parameterized with site observations and driven by satellite observations and meteorological reanalysis products to scale across the region (Mahadevan *et al* 2008, Luus *et al* 2017). PVPRM was initially developed to account for spatial and temporal correla-

tions of carbon exchange with weather and vegetation patterns to use in inverse estimates. It has been a reliable tool for predicting the site level carbon fluxes in various arctic and boreal ecosystems (Luus and Lin 2015, Kwon *et al* 2016, Commane *et al* 2017, Luus *et al* 2017). An updated version of PVPRM using solar-induced chlorophyll fluorescence (SIF) from the Global Ozone Monitoring Experiment-2 (GOME-2) project (Joiner *et al* 2014) as the photosynthetic indicator has shown improved performance compared to vegetation indices based on near-IR reflectance (Commane *et al* 2017). Several studies show that seasonality in GOME-2 SIF observations is tightly correlated with seasonal patterns of gross primary production across a range of Asian and North American flux sites (Joiner *et al* 2014, Ichii *et al* 2017). Also, SIF can accurately capture the short-term variation in photosynthetic activity (the spring onset in particular) by evergreen needleleaf forest, deciduous broadleaf forest, and northern arctic tundra (Walther *et al* 2016, Luus *et al* 2017). However, GOME-2 SIF's capacity to represent photosynthetic activity in larch forests has yet to be adequately evaluated.

In this study, we apply field observations of carbon, water, and energy fluxes over a larch forest located near the southern margin of the Central-Siberian boreal zone (Liu J *et al* 2020), aiming to: (1) Determine the environmental controls on net carbon exchanges; (2) Identify unique ecosystem functional traits of larch forests; (3) Incorporate improved estimates of larch ecosystem function into an analysis of trends in regional carbon budgets. The southern margin of the Central-Siberian biome is experiencing the profound impact of climate change and evolving quickly from the interaction between environmental conditions and larch ecosystems (Esper and Schweingruber 2004, Zhang *et al* 2011). To accomplish the study, we examine the larch's carbon dynamics over the full range of soil freeze-thaw cycles and explore the response of carbon fluxes to major microclimatic variables. We compare site-level phenological observations to GOME-2 SIF products. We apply PVPRM to investigate the unique characteristics of larch ecosystems. Finally, we use PVPRM parametrization as a basis for spatiotemporal extrapolations of the larch ecosystem and compare its calculated carbon budgets with several major boreal forests. The results of this study add new insight into the future state of carbon cycling in high-latitude ecosystems.

2. Methodology

2.1. Site descriptions

China's Mohe (CN-Moh) boreal larch forest site (53°28'02.94" N, 122°20'16.98" E) is situated in the southern edge of the Siberian continuous permafrost region with an active layer thickness of 0.5–1.0 m and an elevation of 290 m above the sea level (Figure 1a; the red triangle). The Mohe walk-up flux tower (dimensions: 36 m height × 2 m wide × 2 m long with total 17 floors) was built in late 2014 and data collection began in late Jan. of 2015 (Liu J *et al* 2020). Mean annual temperature and mean annual precipitation monitored at the Mohe weather station 50 km south from the Mohe tower for 1990–2016 are -4.9 °C and 505

mm, respectively. The soils at Mohe site are Alfisols. Vertical soil profile consists of a surface organic layer (0.05–0.20 m depth), a soil layer (0.20–0.30 m depth), and a deep layer of sandy clay (1.0–3.0 m depth). 0–0.20 m depth total soil carbon stock in 2015 was 2.8 kg C m^{-2}.

Vegetation over a 500 m radius centering on the Mohe tower is dominated by the deciduous needleleaf forest of *Larix gmelinii* Rupr. (Dahurian larch), along with few stands of evergreen needleleaf Mongolian Scots pine (*Pinus sylvestris* var. *mongolica*). Additional details on forest characteristics of the Mohe site are given in Table S1. White birch (*Betula platyphylla*) and aspen (*Populus davidiana*) are common post-fire pioneer deciduous broadleaf species that occur as the dominant species in recent burn scars, or as scattered individuals in otherwise conifer-dominated stands. Local understory vegetation includes ledum (*Ledum palustre*), lingonberry (*Vaccinium vitis-Idaea*), saussurea (*Saussurea japonica*), Dahurian rhododendron (*Rhododendron dauricum*), and blueberry (*V. uliginosum*). Mohe boreal larch forests show obvious phenological cycles within the year (Figure 1c).

Three species of larch are found across eastern and Central-Siberia (Figure 1b): western-distributed *L. sibirica* (Siberian larch), central-distributed Dahurian larch, and eastern-distributed *L. cajanderi* (Cajander larch). Dahurian larch and Cajander larch cover 1.9 and 2.6 million km^2, respectively. Dahurian larch and Cajander larch are closely related species, but they have distinct morphology. Most importantly, Dahuarian larch is a warmer-adapted subtype than Cajander larch (i.e., the cooler-tolerant larch subtype), and has a higher reproductive potential among three boreal larch subtypes (Abaimov 2010).

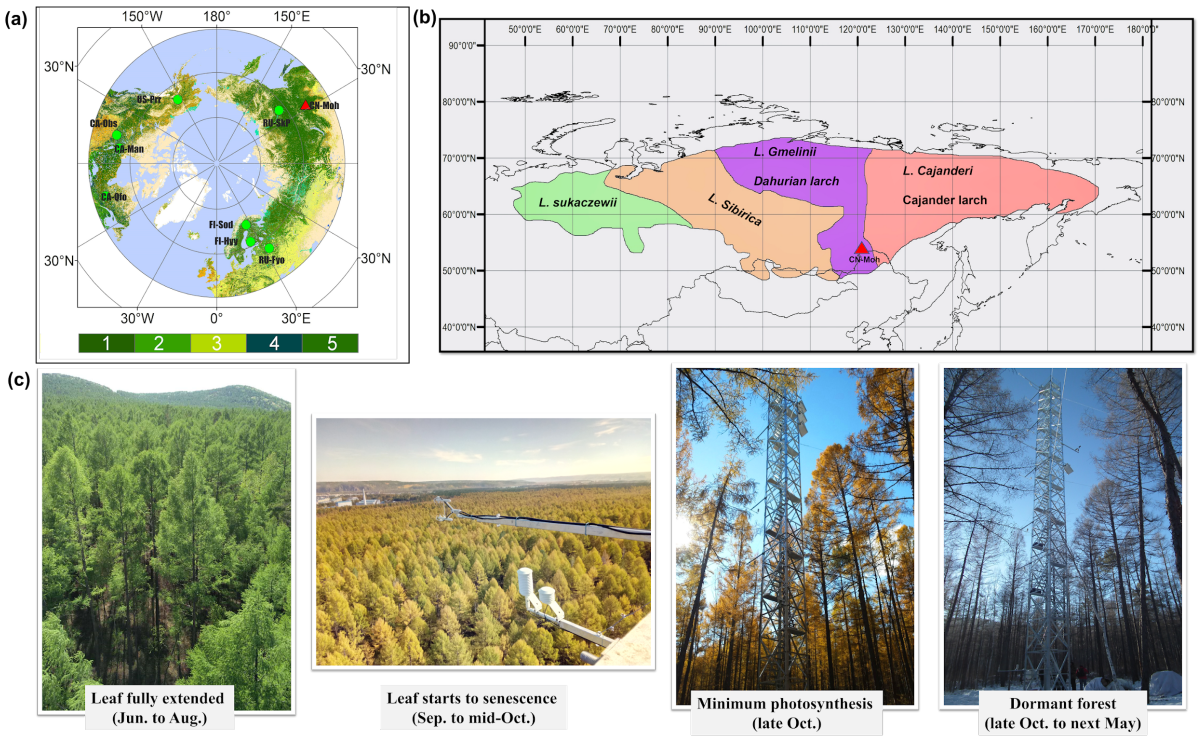

Figure 1. Panel (a): Land-cover map of the boreal-arctic zones (> 45° N). Panel (b): Geographical distribution of Siberian larch species remade from Abaimov (2010). Panel (c): Site photos for different phenological stages. IGBP data was acquired from GlobCover Land Cover Maps processed by European Space Agency and Université Catholique de Louvain (http://due.esrin.esa.int/page_globcover.php). Color legends for IGBP category: (1) Closed to open (> 15%) broadleaf evergreen and/or semi-deciduous forest (> 5 m canopy coverage), (2) Closed (> 40%) broadleaf deciduous forest (> 5 m), (3) Open (15%–40%) broadleaf deciduous forest (> 5 m), (4) Closed (> 40%) needleleaf evergreen forest (> 5 m), (5) Open (15–40%) needleleaf deciduous or evergreen forest (> 5 m). Detailed information about nine identified boreal sites showed through Table S2 (also see Liu J *et al* 2020).

2.2. Climate measurements and analysis

Air temperature, relative humidity, and wind speed were measured at 35 m height on the Mohe flux tower using HMP155 probes (Vaisala, Vantaa, Finland), and 010C wind speed sensor (MetOne, Grants Pass, USA). Photosynthetically active radiation and net radiation were measured at 23 m height by a LI190SB (Li-Cor, Lincoln, USA) and an NR01 sensor (Hukseflux, Delft, Netherlands), respectively. Liquid precipitation was measured at 23 m height using an unheated

tipping bucket rain gauge (TE525, Campbell, USA). Four CS650 integrated soil temperature, moisture, and conductivity probes (Campbell Scientific, Logan, USA) were placed into the ground at 5, 10, 20, and 40 cm depths to measure the profile soil temperatures and volumetric soil water contents 10 m away from the tower. Soil heat flux was measured by two soil heat flux plates (HFP01, Campbell, USA), placed at depths of 10 cm below the surface at eastern and western directions 10 m from the base of the tower adjacent to the west soil temperature profile point. These measurements were sampled with a 5 min interval and saved as 30 min averages by a CR3000 datalogger (Campbell Scientific, Logan, USA). Meteorological station-based, bias-corrected, daily averaged, regional air temperature and shortwave radiation from 2010 to 2014 of Mohe county were downloaded on 30 April 2017 from the China Meteorological Data Service Center. Regional Photosynthetically active radiation (mol m^{-2} s^{-1}) was converted from shortwave radiation using an average factor of 1.98 mol s^{-1} W^{-1} (Mahadevan *et al* 2008).

2.3. CO_2 flux measurement and analysis

An integrated three-dimensional sonic anemometer and open-path infrared gas analyzer, the IRGASON (Campbell Scientific, Logan, USA), was installed on a boom extending 2 m to the north from the railing at the top of the tower to measure horizontal and vertical wind velocity, sonic temperature, water, and carbon dioxide concentrations. The IRGASON signals were stored on a second CR3000 datalogger at 10 Hz (Liu J *et al* 2020). The raw CO_2 measurements by IRGASON have an artifact due to spectroscopic effects (Wang *et al* 2016). Application of the recommended spectroscopic correction for the IRGASON eliminated implausible CO_2 uptake in frozen periods with bare canopy. The net ecosystem exchange (NEE), sensible heat, and latent heat were further derived from these measurements (Baldocchi 2003, Barr *et al* 2006). Valid NEE observations were obtained on Julian day 42–325 in 2015 and 121–205 in 2016. Solar power at the site was insufficient to operate an independent analyzer for measuring the vertical CO_2 concentration profile needed to calculate the storage term. Because the canopy is sparse and the trunk space quite open on account of self-pruning by boreal larches, we assume that the vertical profile for CO_2 is uniform down to a thin layer closest to the ground. By our definitions, negative NEE values represent net carbon flux towards the ecosystem (down), and positive NEE represents net carbon emission towards the atmosphere (up).

We adopt the planar fit method with velocity bias for tilt correction. Turbulent fluctuations were calculated by Reynolds (block) averaging. A 0.13 m s^{-1} friction velocity threshold for Mohe tower was determined by the Moving-Point-Test (Papale *et al* 2006), e.g., approximately 42% of total observed data exceeded the threshold in 2015. Half-hourly flux was calculated by EddyPro (Li-Cor, Lincoln, USA). The footprint of the tower was estimated by a three-dimensional Lagrangian stochastic model (Kljun *et al* 2004), and the maximum distance for 90% influence contour was approximately 900 m. Energy balance closure, evaluated as the orthogonal-regression slope of energy components, was 87%

(Figure S1). The gap-filling method considered both the co-variation of fluxes with environmental variables and the temporal autocorrelation of the fluxes (Falge *et al* 2001, Reichstein *et al* 2005). For flux partitioning, the temperature dependence of the nighttime NEE was quantified and used to project daytime respiration (Reichstein *et al* 2005).

We apply the structural equation model to identify the non-linear complexity of microclimatic controls on NEE. This empirical model is a multivariate method that can process multiple dependent variables simultaneously. Fundamental structures of latent constructs in the model contained primary factors (e.g., radiation and precipitation) and secondary factors (Fyllas *et al* 2017, Luo *et al* 2017), where we assume that primary factors were essential driving factors for the ecosystem, and the secondary factors were thus controlled by them.

2.4. PVPRM parameterization

In PVPRM, NEE is modeled as the sum of gross primary production (GPP) and ecosystem respiration (R_e), as shown in Figure 2a. GPP is calculated based on observed temperature (T_{obs}), radiation (PAR), and a phenological index (SIF) derived from satellite observations. GOME-2 SIF was normalized by the cosine of the solar zenith angle to account for the intensity of surface irradiance at the time of measurement. R_e is estimated as a linear function of temperature residuals (ΔT). ΔT equals to T_{obs} – T_{min} (i.e., the minimum temperature; set to -10 °C) if $T_{obs} > T_{min}$, and ΔT will be zeroed if T_{obs} T_{min} in long harsh winters. PAR_0 represented the half-saturation value of photosynthetically active radiation (the PAR), and stood for the light use efficiency. The temperature scalar (T_{scale}) is calculated as the difference of T_{min} and the maximum temperature thresholds for the photosynthesis (T_{max} = 40 °C; Figure 4 in Wang *et al* 2008), and including a regulator of optimal photosynthetic temperature (T_{opt} = 20 °C; Figure 3 in Quan *et al* 2018).

VPRM parameterization only used the unfilled half-hourly NEE because gap-filling algorithms would bias the result by imposing a separate modeled functional relationship (Luus and Lin 2015). Therefore, observed flux data from 2015 were used for parameterization, and data from a short period of 2016 were applied for model evaluation. Further, carbon budgets from 2010 to 2014, which represented the baseline of larch forest on the southern border of central Siberia were then extrapolated based on simulated PVPRM parameters, regional climatic observations, and satellite photosynthetic indicator (i.e., GOME-2 SIF).

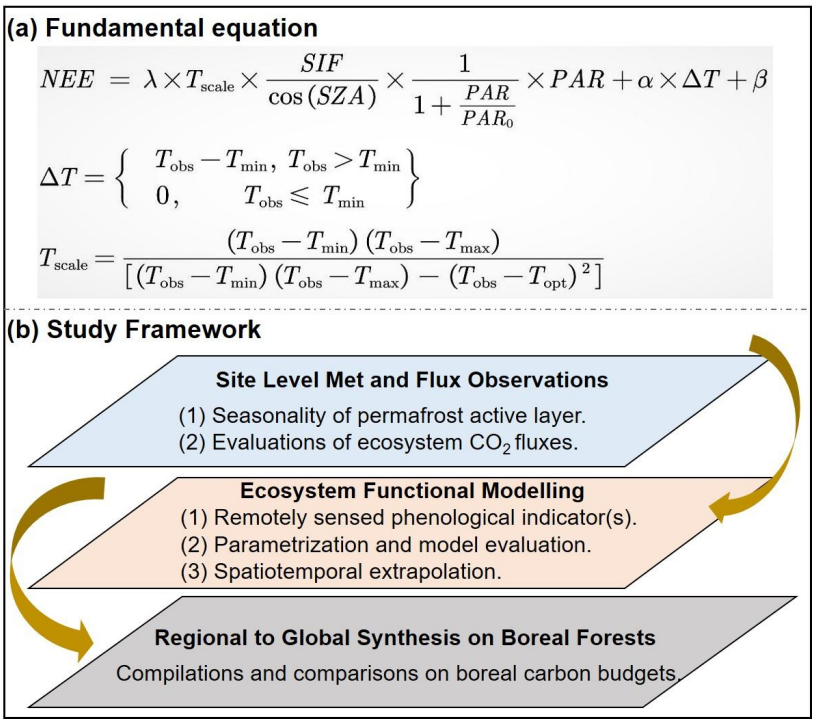

Figure 2. Schematic of PVPRM structure and study framework.

3. Result and discussion

3.1. Permafrost seasonality and observed ecosystem CO_2 exchanges at Mohe sites

Soil freeze-thaw states at Mohe site were identified by asynchronous patterns of soil temperatures in two soil layers (surface 5 cm and deep 40 cm), including periods of frozen soil, soil freeze-thaw transitions, and thawed soil (Figure 3, Table S3). We observe the zero-curtain effect at Mohe site, which has been reported to influence soil processes at tundra sites as well (Zona *et al* 2016). The effect results from latent heat buffering soil temperature near 0 °C for a period while soil water freezes or thaws (Outcalt *et al* 1990). At the Mohe site, the zero-curtain effect existed only for 7–10 days in the early spring.

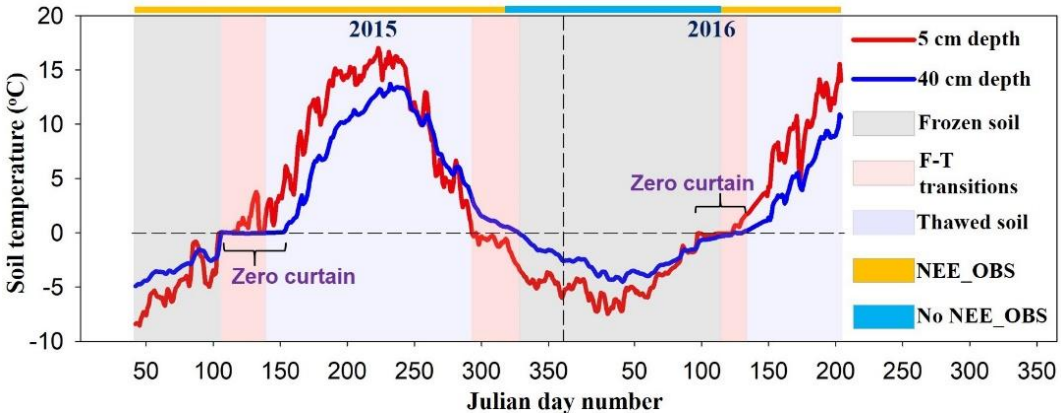

Figure 3. Soil freeze-thaw status in Mohe site defined by two layers of soil temperatures. Periods of frozen soil, freeze-thaw transition, and thawed soil were indicated by different color shading. NEE_OBS indicates periods with flux observations, and No NEE_OBS indicates periods that measurements were suspended due to instrument failures and insufficient solar power. Frozen soil stage (grey/black) is defined by soil temperature < 0 °C to at least 40 cm. Freeze-thaw transition (red) is defined as having soil temperature > 0 °C in one layer and < 0 °C in the other. The thawed soil period (blue) is defined by soil temperature > 0 °C from the surface to at least 40 cm depth.

Carbon uptake at Mohe increased gradually as temperature increased (Figure 4a, Table S2). NEE was slightly negative around noon (i.e., periods with high radiation) during freeze-thaw transition seasons (Figure 4d). Carbon assimilation during the spring thaw is driven by other vegetation as the Dahurian larch has not yet produced needles for the year. Other evergreen trees such as Scots pine and early-spring perennial shrubs (e.g., Dahurian rhododendron, lingonberry, etc.) are adapted to respond to the spring soil thaw and regain photosynthetic capacity quickly. Also, NEE at Mohe was very sensitive to changes in near-surface temperature and humidity (Figure S3). This is consistent with experiments and observations from boreal evergreen ecosystems in which their carbon balances are easily affected by microclimatic variabilities (Jarvis *et al* 1997, Zhang *et al* 2006, Ueyama *et al* 2013).

GPP and R_e both increased rapidly from the frozen soil period to the thawed soil period (Figure 4e–g, Table S4). GPP increased more rapidly than R_e. R_e persisted at a low rate (~0.68 mol m^{-2} s^{-1}) even during periods with fully frozen soil (magnitudes given in Table S4), suggesting that microbes (or roots) are tolerant of temperatures below 0 °C or exist in microsites that are protected from freezing (e.g., by concentrated salt solutions or antifreeze compounds). Natali *et al* (2019) show that winter soil carbon loss is greater than summer carbon uptake in the northern permafrost domain. Alternatively, CO_2 that was generated at depth before the active layer completely froze could be slowly

diffused through the frozen soil layers (Figure S2), as indicated by Wang *et al* (2013) observation that snowpack on the forest floor but not the frozen soil act as the decisive factor affecting permafrost soil respiration.

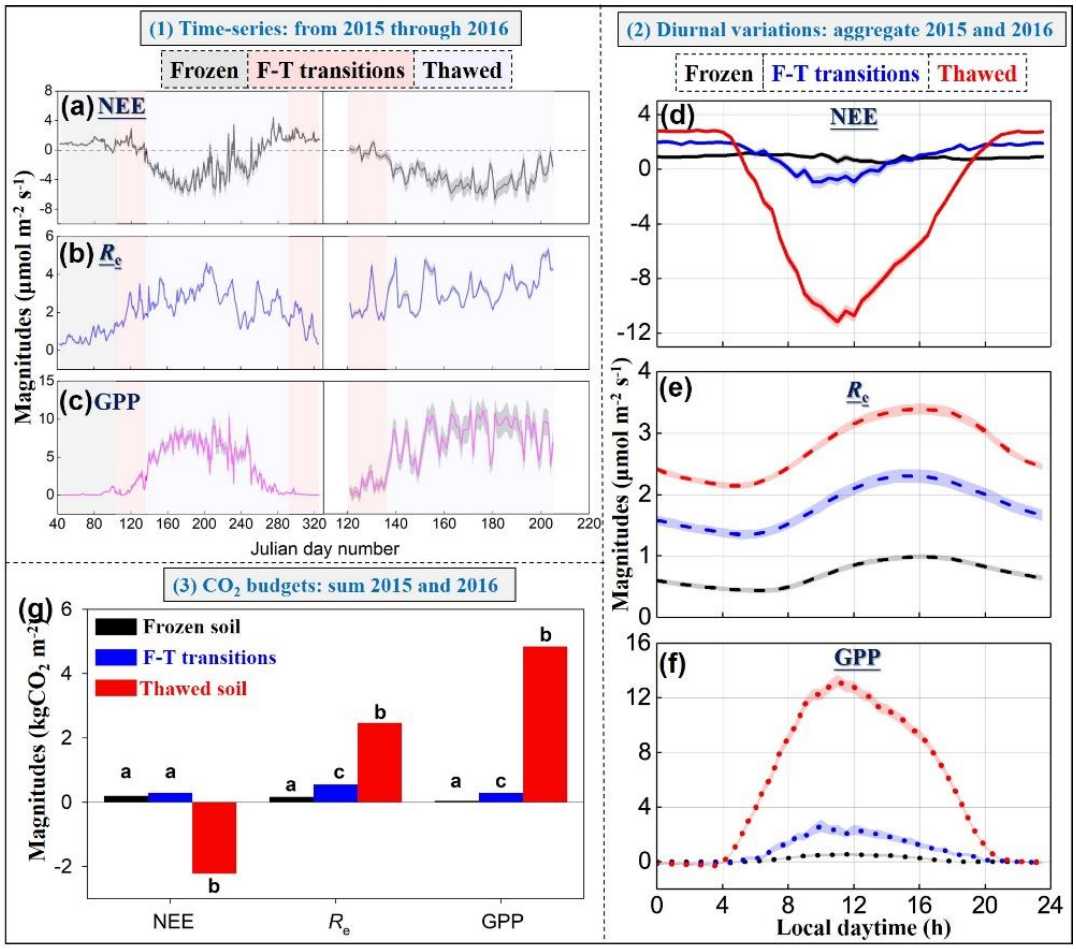

Figure 4. Grouped panels (1) Time-series variations, (2) cumulative budgets, and (3) diurnal variations of gap-filled CO_2 fluxes at Mohe site. NEE, R_e, and GPP are net carbon fluxes, ecosystem respiration, and gross primary production, respectively. The shaded area indicates standard errors (± s.e.). In panel (g), variables with the same letters in each group of variables were not statistically different (p 0.05) or with different letters were significantly different ($p <$ 0.05), according to Duncan's multiple range test. Unit of fluxes have been switched in (g) for the annual budget and reported in kilogram CO_2 per m².

Micro-climate at the southern margin of Central-Siberia differs from other cir-

cumpolar ecozones, especially tundra and boreal evergreens in several key features. (1) Distinct seasonality of below-ground permafrost active layer (Guo *et al* 2018). Soil-air energy transfer was important mechanistic feedback between soil carbon emission and physical status in the ecosystem. The zero-curtain effect hasn't been reported in boreal evergreens sites so far. But in the tundra, the zero-curtain effect usually lasts for nearly a month per year, with a week in spring but evidently longer in autumn (Zona *et al* 2016). At Mohe, short spring zero-curtain is observed for both years, but autumn zero-curtain is not obvious (i.e., 40 cm soil temperature is relatively stable for several days while surface soil temperature is decreasing rapidly). This is possible because of the earlier and thicker snow cover and higher atmospheric temperature in the region. (2) Distinct seasonal patterns for above-ground heat flux (Bonan *et al* 1992, Betts and Ball 1997). Dahurian larch forest has high albedo in winter when the canopy is bare and the snow-covered ground is exposed to the sky, whereas the albedo of evergreen forest remains low in winter because the dark canopy obscures the snow-covered ground except when intercepted snow coats the branches. (3) Limitations of ecosystem water availability (Peng *et al* 2011, Way *et al* 2013). As we observed a larger path coefficient value attached to the variable of precipitation at the Mohe site via the structural equation model, so that precipitation ('ecosystem water availability') would be the essential limitation to Dahurian larch's carbon assimilation capacity. This is likely because the final position of water table depth would strongly influence the carbon balances by directly controlling soil freeze-thaw processes (Dunn *et al* 2007) and indirectly affect bacteria and microbial activities at anoxic-oxic interfaces (Reim *et al* 2012).

3.2. Dahurian larch's unique functional traits

We assessed SIF is a reliable indicator for short-term variations in canopy activity at the Mohe site (Figure 5). SIF is available at higher time resolution (daily) than EVI, but it has coarse spatial resolution compared to MODIS, which makes it not as good to capture the spatial variability (Shen *et al* 2014). It is worth noting that SIF's retrieval method (i.e., Fraunhofer line) is insensitive to earth surface disturbances (Joiner *et al* 2014). However, the benefit of EVI's high spatial resolution is offset by data loss due to atmospheric scattering and variable surface reflectance (Walther *et al* 2016), especially in the remote Siberia which has more frequent clouds than other regions (i.e., the Siberian Anticyclone).

We examined the light response of daytime NEE and temperature dependency of R_e at the different soil freeze-thaw states (Figure S4). Interactions of temperature and radiation on NEE were also tested by multiple regression analysis (Figure S5), which showed that half-hourly unfilled NEE was sensitive to this interaction under all soil freeze-thaw states. The effect of radiation on daytime NEE gradually increased from frozen soil to thawed soil periods. During days of frozen soil and freeze-thaw transitions, soil temperatures have a stronger influence on R_e than air temperature does (Figure S4g, h). While the air temperature only appeared to be a better temperature parameter for the PVPRM

fitting during thawed soil periods (Figure S4i). The result indicated further that in cooler days especially when Dahurian larches were not yet able to photosynthesize, soil respiration (e.g., heterotrophic by microbes or autotrophic by roots) was dominating the R_e. However, in warmer days when the needles had emerged, above-ground respiration (i.e., leaf autotrophic respiration) became a larger component in R_e. As Hermle *et al* (2010) assesses that heterotrophic and autotrophic respirations contributed equally to R_e in spruce forest. Thus, these interannual interactions and dynamic distributions of R_e subcomponents are less studied but are critical for evaluating Dahurian larch's carbon budgets (Pries *et al* 2013).

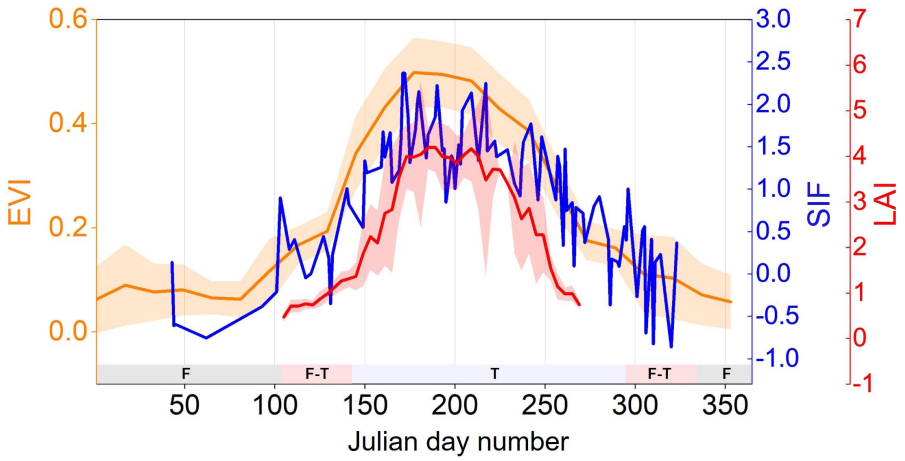

Figure 5. Comparisons of different phenological indexes at Moh site in 2015. 16-day MOD13Q1 Enhanced vegetation index (EVI; unitless; every 16-day) was upscaled to 40-km spatial resolution. Daily GOME-2 solar-induced chlorophyll fluorescence (SIF; units in mW m^{-2} nm^{-1} sr^{-1}; every 1-day) was originally in 40-km resolution. Leaf area index (LAI; unit in m^2 m^{-2}; every 3-day) was measured *in situ* by an LAI-2200c instrument (Li-Cor, Lincoln, USA). LAI is the average of 30 observations made at sampling positions within 100 m of the Mohe tower from mid-April to late September in 2015. Periods of permafrost seasonality, such as frozen soil (F), freeze-thaw transitions (F-T), and thawed soil (T), are given along with the Julian day number. The shaded area indicates ± 1 s.d.

PVPRM parameters are intended to account for the major functional relationships that regulate carbon exchange by an ecosystem (Table 1). Light use efficiency ( ) for the Mohe site was 0.02 ± 0.003 [(mol CO_2 m^{-2} s^{-1})/(mol PAR m^{-2} s^{-1})]. Half-saturation radiation for photosynthesis (PAR_0) was 807 ± 61 mol m^{-2} s^{-1}. The linear temperature response for ecosystem respiration is represented by (0.03 ± 0.004 mol CO_2 m^{-2} s^{-1} $^oC^{-1}$) and (1.05 ± 0.1 mol CO_2 m^{-2} s^{-1}). For a rational comparison, we adopted a series of R_e from various

boreal forests (Mahadevan *et al* 2008, Luus *et al* 2015, Luus *et al* 2017), as different forest might adopt diverse $T_{\min}$ settings for optimal parameterizations. R_e near typical minimum temperature in Dahurian larch is usually higher than that of boreal spruces and tundra. Soils microbial community, organic content, and physical properties (e.g., moisture, moss insulation, etc.) at different sites possibly account for those discrepancies (Peng *et al* 2015; Meyer *et al* 2017; Zhong *et al* 2017). Also, PVPRM predictions account for ~80% of the variation in the training data (Figure S7a; Table S5), while the explanatory ability was slightly reduced for the evaluation data (Figure S7b). We find PVPRM predictive capacity was well correlated with inter-annual precipitation variables at the Mohe site (Figure S8; Table S6). Especially, 2016 had an anomalous dryer (and warmer) soil freeze-thaw transition period compared to 2015 (Table S7). Consequently, simulated NEE magnitudes for this specific period was lower than our observations (Table S8).

Table 1. Fundamental parameters and key statistics for the PVPRM parameterizations. Input data was half-hourly unfilled observations from 2015. The air temperature was adopted for the modeling since soil temperature is less sensitive to the controlling of R_e (Figure S4). Units were: PAR_0 in mol m^{-2} s^{-1}; λ in (mol CO_2 m^{-2} s^{-1})/(mol PAR m^{-2} s^{-1})(mW m^{-2} nm^{-1} sr^{-1}); α in mol CO_2 m^{-2} s^{-1} $^oC^{-1}$; β in molCO_2 m^{-2} s^{-1}. According to the original equations (Mahadevan *et al* 2008) and our model settings (Figure 2a), β well represents the maximum light efficiency for phenological peak and temperature optima at the Mohe site, and α can be considered as the indicator linking with the magnitude of soil organic carbon pool plus the supply of substrate from roots.

PAR_0	λ	α	β	σ-PAR_0	σ-λ	σ-α	σ-β	RMSE
807.3	-0.02	0.03	1.05	61.0	0.0	0.0	0.1	3.8

3.3. Spatial-temporal extrapolation of carbon budgets at Mohe site

PVPRM parameters optimized for Mohe were applied here to investigate how climate variability would have influenced the regional carbon budget from 2010 to 2014 in Dahurian larch (Figure 6). We examine environmental variations in the PVPRM driving forces (where air temperature, radiation, and phenological status were binned by annual totals) from 2010 to 2014. Air temperature ($F_{4,\ 1827} = 4.7$) was comparable ($p > 0.05$) over the period, while radiation ($F_{4,\ 1827} = 5.8$) and SIF ($F_{4,\ 1827} = 3.3$) were markedly different ($p < 0.05$) among the years. Analysis revealed that the SIF ($R^2 = 0.79$) had a stronger influence on PVPRM predicted NEE than radiation ($R^2 = 0.73$) or air temperature ($R^2 = 0.62$). GOME-2 SIF is sensitive to photosynthetic capacity. Warm temperatures or high radiation inputs that occurred when SIF was low were not utilized by the forest. The spatial representativeness and accuracy of PVPRM are limited

by the resolution of weather data (i.e., site level) and spatial and temporal resolution of the SIF products (i.e., ~40 km) that account for phenology and spatial patterns in vegetation density and status.

The annual regional climate during 2010–2014 was comparable to 2015 (Figure S9). Modeled patterns and sums of NEE and GPP showed significant inter-annual variabilities. On the contrary, both patterns and sums of R_e were consistent across years. Because the model only includes temperature control of R_e and air temperatures were relatively constant among the years there is little difference in simulated R_e (e.g., Figure S10b). Differences of GPP were because of inter-annual variations of regional radiation and satellite phenological indicators (Figure S10c). Consequently, we imply the intra-annual NEE differences estimated by PVPRM were mostly driven by GPP variations as R_e was constant.

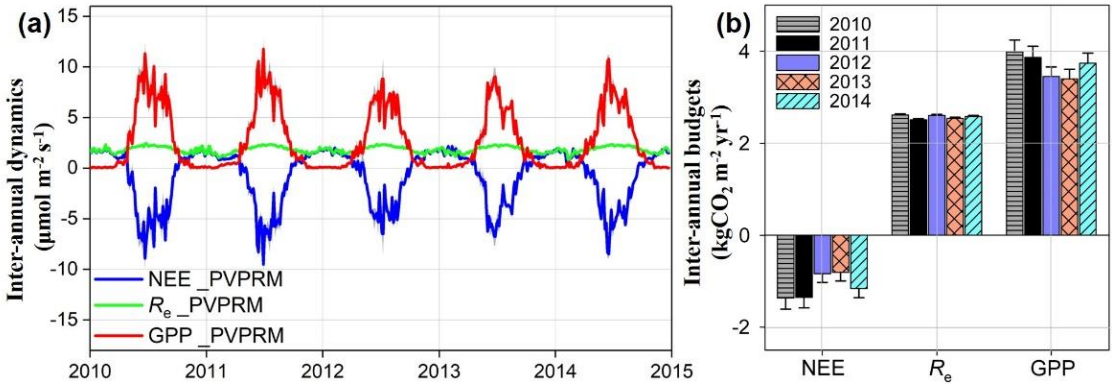

Figure 6. Panel (a) Time series of 4-day averaged NEE, R_e, and GPP predicted by PVPRM trained with 2015 Mohe data shows relatively constant R_e but the distinctly different magnitude of peak NEE and GPP among the years. Panel (b) Annual sums for NEE, R_e, and GPP for each year of 2010-2014. The s.e. in panel (b) come from Monte-Carlo simulation (by generating an array of estimates and calculating associated uncertainties). Annual sums of R_e are not significantly different ($p > 0.05$), while differences of NEE and GPP across years are significant ($p < 0.05$).

3.4. Comparisons of carbon budgets among multiple boreal forests

We find most boreal forests that have been studied were net carbon sinks (Table 2). CA-Qfo, which is carbon neutral, and RU-Fyo and FI-Sod, which have been net carbon sources since 2014, were the only exceptions. These are site-level comparisons, so that extrapolation to the entire boreal-arctic zones again has large uncertainties as discussed above. The results predict ranking amongst the vegetation types that can be tested with additional data that quantifies the magnitude of inter-site variability for each ecosystem type. These flux observations are the best available tool to date for exploring northern ecosystem

carbon-water-energy exchanges and climate change responses (Baldocchi *et al* 2001). Inferences from the site data provide a reference for evaluating and correcting satellite-based land-atmosphere flux products (e.g., MODIS, AVHRR, ISLSCP- , and GOME-2; Turner *et al* 2006, Fisher *et al* 2008, Joiner *et al* 2014).

Further, we find that sites dominated by Siberian larches (Dahurian + Cajander) have a stronger annual carbon sink than either pine or spruce dominated forests (Figure 7). Larch forest has the highest GPP with a low R_e, which results in a larger annual uptake. Spruce forest is a weaker carbon sink because of the lowest GPP but higher R_e. While the highest R_e of pine forest largely offsets its strongest GPP. Reported site-level observations of soil carbon stocks were 5.02 $\pm$ 0.74 (mean $\pm$ s.d.) kg C m^{-2} for pine (0–50 depth; averaged from four chronosequence sites near FI-Hyy; Kolari *et al* 2004), and 4.43 $\pm$ 2.53 kg C m^{-2} for spruce (mineral soil; averaged from CA-Qfo, CA-Obs, and CA-Man; Bergeron *et al* 2007), while only 2.76 kg C m^{-2} for the Dahurian larch (0–20 depth at CN-Moh). We see most organic carbon accumulated in surface soils at the Mohe site, and below 30 cm soil is mixed with sand, clay and rock. Consequently, on a regional scale, the ranking of R_e across boreal species domains (larch $<$ spruce $<$ pine) are correlated with the size of soil carbon stocks, where a larger carbon pool usually had a greater potential decomposition rate ($r = 0.48$, $p < 0.05$; Table 2).

Climate change affecting boreal ecosystem health and stability has been a prolonged focus (Shuman *et al* 2011). The temperature sensitivity of respiration is often expressed as the Q_{10}, which indicates how much R_e will increase for a 10 °C temperature increase (Meyer *et al* 2017). Q_{10} values were directly identified from the partitioned flux observations of each boreal site in a longer temporal scales (i.e., 3–18 yr intervals), to track the actual physiological responses instead of seasonal changes in substrate input and phenological changes in in depth of active layer. Specifically, Q_{10} in CA-Qfo, CA-Obs, and CA-Man were collected from the literature (Bergeron et al 2007), while all others were derived from the flux measurements by using R *respirometry* package (Table 2). We see Q_{10} differed between ecosystems with a much stronger response in the spruce forest compared to that of pine or larch (Figure 7d; Table 2). Spruce ecosystems can access deeper peat layers when exposure to the warmer climate (Dunn *et al* 2007). The Q_{10} differences between deciduous and evergreen forests in part revealed their ecosystem functional traits in acclimating to the distinct environments. For instance, when the surrounding temperature becomes low, and radiation becomes weak, deciduous larch will shed all leaves and enter dormant status. But pine and spruce still have metabolic costs through the transition seasons to maintain their foliage and provide it with protection from frost damage during winter dormancy (Sutinen *et al* 1992).

Table 2. Statistics of annual carbon budgets over different boreal sites. Data downloaded on July 30th, 2017 from FLUXNET2015 Tier One (Table S2), and reported in formats of mean $\pm$ s.e. Q_{10}

stands for the temperature sensitivity of ecosystem respiration (R_e). Soil organic carbon (SOC) data were retrieved from the Global Soil Organic Carbon Map (http://54.229.242.119/GSOCmap/). Mean SOCs were calculated based on an approximately 50 km^2 pixels by centering the flux tower.

Geolocation	Site name	Data periods	Flux years	SOC (Mg ha^{-1})	NEE (kgC m^{-2} yr^{-1})	R_e (kgC m^{-2} yr^{-1})	GPP (kgC m^{-2} yr^{-1})	Q_{10}
Alaska	US-Prr	2011–2014	4	77.36 ± 43.61	-0.11 ± 0.03	0.36 ± 0.06	0.44 ± 0.05	1.6
Canada	CA-Man	1994–2003 2006–2008	13	102.11 ± 33.68	-0.03 ± 0.02	0.68 ± 0.03	0.71 ± 0.03	3.8
	CA-Obs	2000–2010	11	101.26 ± 29.04	-0.04 ± 0.01	0.80 ± 0.02	0.84 ± 0.02	3.0
	CA-Qfo	2004–2010	7	102.36 ± 16.91	0.00 ± 0.01	0.65 ± 0.02	0.65 ± 0.02	2.8
European Russia	RU-Fyo	1998–2014	17	99.13 ± 51.37	0.14 ± 0.03	1.62 ± 0.06	1.44 ± 0.05	2.0
Scandinavia	FI-Sod	2001–2014	14	77.50 ± 32.60	0.10 ± 0.01	0.72 ± 0.02	0.63 ± 0.02	2.2
	FI-Hyy	1997–2014	18	81.65 ± 35.67	-0.21 ± 0.01	0.90 ± 0.01	1.16 ± 0.02	2.2
Siberia	RU-SkP	2012–2014	3	63.94 ± 27.72	-0.21 ± 0.01	0.23 ± 0.07	0.50 ± 0.08	1.5
	CN-Moh	2010–2014	5	107.60 ± 47.02	-0.30 ± 0.03	0.70 ± 0.00	1.01 ± 0.03	1.3

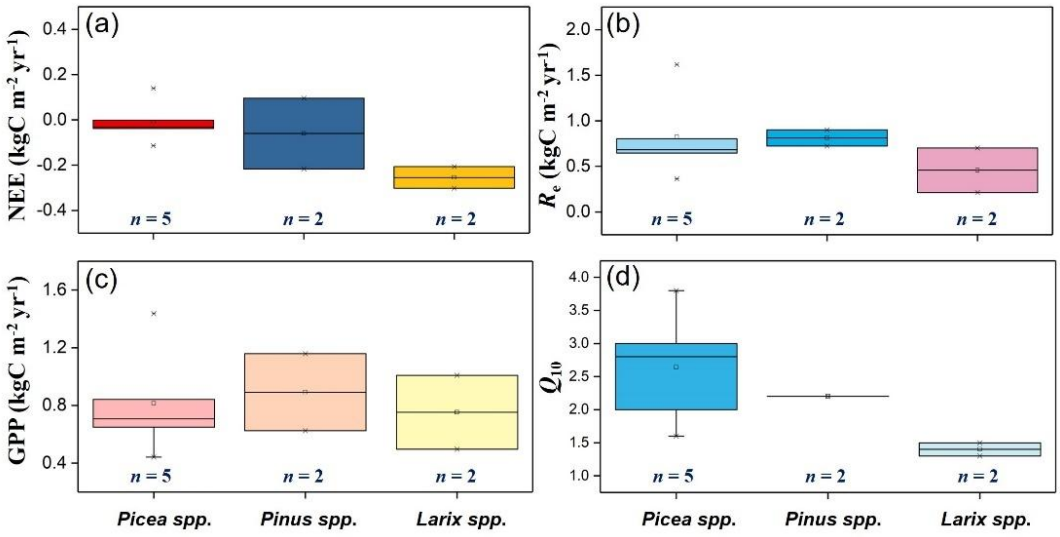

Figure 7. Comparisons of annual carbon budgets and respiratory temperature sensitivity grouped by different species domains, including *Piceas abies* (Norway spruce), *Picea mariana* (black spruce), *Pinus sylvestris* (Scots pine), *Larix cajanderi* (Cajander larch), and *Larix gmelinii* (Dahurian larch).

3.5. Comparisons of carbon budgets in Dahurian and Cajander larches

The analysis revealed a potentially stronger carbon sink of Dahurian larch growing in the ecotone than for larch subtypes growing in the interior Siberia. The carbon fixation at CN-Moh is larger than RU-SkP (Table 2, which is in the interior of Siberia where Cajander larch dominates). The two sites have not

only different mean annual temperature and precipitation (Table S2), but also distinct forest characteristics. While on the other hand, two sites differ by 9^{o} latitude, averaged summertime (i.e., June, July, and August) solar radiation input (Moh 37.8 MJ m^{-2} d^{-1} and SkP 36.3 MJ m^{-2} d^{-1}) are similar. Then we proposed a simplified scenario to test separate contributions from Dahurian larch and Cajander larch to Siberian forest's carbon budgets. Zhang *et al* (2011) found climate-change induced ecosystem shift could lead to the warmer-adapted Dahurian larch gradually replacing the cooler-tolerant Cajander larch. As shown in Table 3, the extrapolated NEE by Cajander larch to the Siberian boreal forest only will leave a net carbon pool of 0.26 ± 0.02 PgC yr^{-1}. Alternatively, NEE by Dahurian larch only will leave an increased net carbon pool to 0.37 ± 0.01 PgC yr^{-1}. By assuming the actual Siberian forests consist of 35% Dahurian larches and 48% Cajander larches (Abaimov 2010), the net annual carbon exchange should be at least 0.31 ± 0.08 PgC. However, the previous well-known inventory reported a 0.26 PgC pool for the entire Siberian forests (Pan *et al* 2011). This bottom-up inventory ignored Dahurian larch due to data limitations at that point.

However, the difference between two approaches (0.05 PgC) is smaller than scenario's uncertainty (0.08 PgC). Because our simplified scenarios exclude the accelerated rate of permafrost degradation and intensified frequency of regional wildfires (Sala *et al* 2000, Esper and Schweingruber 2004, Bonan 2008, Schuur *et al* 2009, Tchebakova *et al* 2009, Shuman *et al* 2011, Gauthier *et al* 2015). Also, we recognize there is considerable uncertainty in extrapolating from southern-edged Dahurian larch to its northern biomes. Spatial heterogeneity, inter-species differences, and intra-species dynamics are still inadequately accounted for in this study and other similar studies due to data limitations for the vast Siberia (Litvak *et al* 2003; Miles and Esau 2016; Villarreal *et al* 2018). Synthesis across the available data from field measurements in Siberia provides an emerging result that ecosystem functional types and contributions to boreal-arctic carbon cycles of larch forest may be underrepresented and underestimated (Nakai *et al* 2008, Shuman *et al* 2011, Zhang *et al* 2011, Ohta *et al* 2014, Takata *et al* 2017, Pan *et al* 2011, Natali *et al* 2019, Liu J *et al* 2020, Liu Z *et al* 2020). We still emphasize that the full range of Siberian carbon sinks would be better defined by including Dahurian larch.

Table 3. Scenarios on estimating Siberian Forest carbon budgets. Total area of boreal larch forests in Siberia was estimated as 150.0 Mha (GlobCover Land Cover Maps), and the total area of Siberian forests was 676.6 Mha (Pan *et al* 2011). 83% Cajander larch scenario assumes 83% of Siberian forests are occupied only by the northern Cajander larch, the same settings as the 83% Dahurian larch scenario. Siberian boreal larch forests consist of 35% Dahurian larches and 48% Cajander larches (Abaimov 2010). ¶Bottom-up carbon budgets of the entire Siberian boreal zone were reported in accordance with Pan *et al* 2011. *ND* is no data. Uncertainty (1 s.d.) is calculated using Monte-Carlo simulations.

Simplified scenarios	NEE (Pg C yr^{-1})	Re (Pg C yr^{-1})	GPP (Pg C yr^{-1})
83% Cajander Larch (CL)	-0.26 (0.02)	0.29 (0.03)	0.62 (0.03)
83% Dahurian Larch (DL)	-0.37 (0.01)	0.87 (0.02)	1.26 (0.02)
48% CL + 35% DL	-0.31 (0.08)	0.53 (0.09)	0.89 (0.11)
Siberian boreal forests¶	-0.26	*ND*	*ND*

3.6. Factors affecting carbon dynamics in boreal forests

The younger forests fix less carbon but respire even less, resulting in net carbon uptake (Figure 8a), and older boreal forests are net carbon sources because they respire more than they accumulate (Litvak *et al* 2003). We find R_e and GPP are larger for forests with a higher mean annual temperature (Figure 8b–c). This may be related to the site latitude, where sites in the warmer and lower latitude usually have the longer growing seasons. Forkel *et al* (2018) showed that GPP is more sensitive to warming than R_e for northern ecosystems in recent decades. However, our results showed both R_e and GPP increased with air temperature, the sensitivity of R_e was even slightly higher than GPP (slopes: $0.07 > 0.05$). We were also aware that comparing these mean conditions at a range of boreal sites is different from investigating interannual variations with environmental alterations at one fixed site. Despite the potential limitations for comparing carbon balances at individual sites with different climates and stand history, there is a clear indication that deciduous conifers that dominate in Siberia exhibit carbon budgets and ecosystem properties that are distinct from the evergreen conifers that have been more thoroughly studied.

Unbalanced photosynthetic accumulations and respiration losses are commonly observed in the boreal zone (Liu Z *et al* 2020). Declining net carbon accumulation with age that we observe was very much consistent with the general trend suggested by Odum (1969). The ecological secondary succession incorporated into the ecosystem development theory was the most common explanation for the declining trend (Mac *et al* 2008, Liu and Randerson 2008). The old-growth boreal forest might transition into the late-successional stage (Curtis and Gough 2018), where their net annual carbon balances will finally move to positive ranges (Figure 9a, Table S9). Aging boreal forests may still be significant carbon sinks (or maybe neutral as was observed at BOREAS NOBS; Glulden *et al* 1998) due to their considerable live wood tissues (Sebastiaan *et al* 2008) and tendency to accumulate woody debris and soil carbon (Kolari *et al* 2004). But carbon storage in boreal forest is often balanced by periodic disturbances, for instance, the wildfire. Predictions of increased fire frequency will alter regional carbon balances and ultimately cause a decline in boreal forest carbon stocks (Bjorkman *et al* 2018). Thus, the age-dependency and wildfire disturbances in boreal zone remains an open question (Conard and Ivanova 1997, Esper and Schweingruber 2004, Carpino *et al* 2018; Biskaborn *et al* 2019; Hart *et al* 2019), particularly, in the Siberian boreal forest with coarse spatial and temporal coverage.

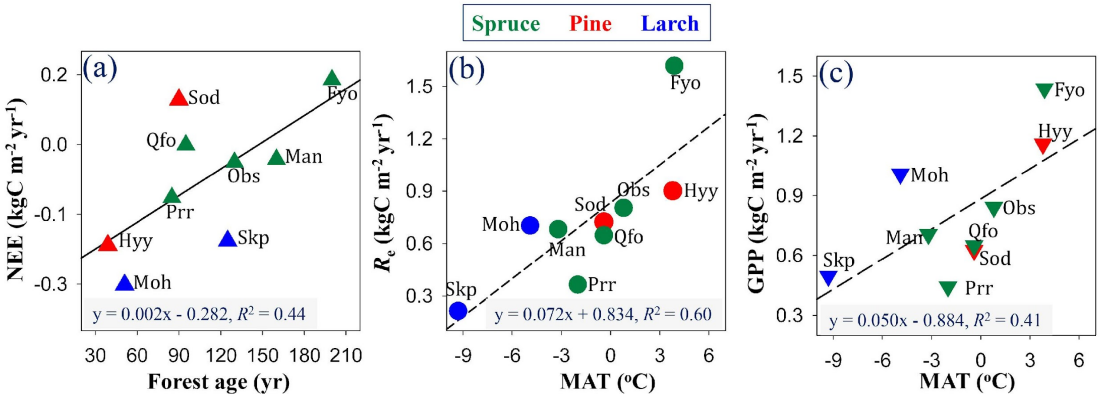

Figure 8. Regression analysis between subcomponents of ecosystem carbon budgets and forest age or the mean annual temperature (MAT) over nine boreal sites. Red, green, and blue colors represent boreal pines, boreal spruces, and boreal larches, respectively. All regressions were significant at the level of $p < 0.05$.

4. Conclusion

We investigated the characteristics of net carbon exchange and its response to microclimate within a boreal Dahurian larch forest site ('Mohe') in the rarely studied southern ecotone region of Siberia using both flux measurements and an empirical ecosystem function model ('PVPRM'). We found that the net carbon balance of our larch stand was regulated closely by the seasonality of the permafrost active layer, air temperature and humidity, and soil water availability. The carbon flux observations at the Mohe site suggested a larger variability in net carbon exchange and a stronger spatial heterogeneity within the Siberian larch biome. We found satellite SIF was a reliable phenological indicator in capturing the timing for the onset of photosynthetic capacity during the early spring needle expansion in Dahurian larch forest. PVPRM parameterization quantified important ecosystem functional parameters from Dahurian larch forests that were distinct from other forest biomes. We saw PVPRM predictions in Dahurian larch forest would be biased if dealing with anomalous precipitation events. Eddy covariance and environmental measurements with longer temporal scales that include a range of precipitation scenarios are needed for improving predictions of carbon budgets across this biome. The impact of environmental extremes, as well as natural disturbances such as wildfires, are key uncertainties that need to be resolved in Dahurian larch forest.

The results presented here for the Mohe Dahurian larch together with previously reported flux data from the Cajander larch site in the interior of Siberia suggested that larch ecosystems provide larger annual carbon sink than other boreal evergreen sites typically found in North America and Fennoscandia. Contributions of boreal larch forest to regional and global carbon budgets were stronger

than had been previously recognized (particularly by Pan *et al* 2011). Inadequately accounting for boreal larch carbon uptake magnitude could result in a low-bias for boreal-arctic carbon budgets. Our results implied that regional carbon sink by Siberian larch would increase if climate warming gave the warmer-adapted larch subtype a competitive advantage that enabled it to replace the cooler-tolerant larch subtype from the margin to the interior Siberia. The measurements established at the Mohe site were a major step toward expanding the observation network and increasing scientific cooperation to better understand the ecosystem's functional traits and carbon dynamics in the vast Siberian larch biome as it responded to climate change. We recommend increasing spatial and temporal coverage in the Siberian boreal zone, to reduce uncertainty in estimates of the current and future circumpolar carbon emissions and budgets.

Acknowledgments: We thank Dr. Archana Dayalu (Atmospheric and Environmental Research) for the assistance and useful discussion in the modeling section.

Declarations: The authors declare no conflict of interests.

Funding: The work is funded by National Natural Science Foundation of China for Young Scholar (32101326), Natural Science Foundation of China (31770488), Initiative Programme for Young Scholar of Shanghai Academy of Landscape Architecture Science and Planning (KT00257), Shanghai's Science and Technology Innovation Action Plan (20DZ1204802), and Research fund of Shanghai Landscaping and City Appearance Administrative Bureau (G190201).

Open research: Raw and processed flux data and meteorological measurements for CN-Moh, including the R based PVPRM codes, are all openly downloadable at https://doi.org/10.7910/DVN/VGNMQP. This work also used flux data acquired and shared by the FLUXNET community (https://doi.org/10.1038/s41597-020-0534-3), including these networks: AmeriFlux, AfriFlux, AsiaFlux, CarboAfrica, CarboEuropeIP, CarboItaly, CarboMont, ChinaFlux, Fluxnet-Canada, GreenGrass, ICOS, KoFlux, LBA, NECC, OzFlux-TERN, TCOS-Siberia, and USCCC.

References

Abaimov, A. P. (2009). Permafrost Ecosystems, Siberian Larch Forests. *Ecological Studies*, 41–58. https://doi.org/10.1007/978-1-4020-9693-8_3

Bakwin, P. S., Jacob, D. J., Wofsy, S. C., Munger, J. W., Daube, B. C., Bradshaw, J. D., et al. (1994). Reactive nitrogen oxides and ozone above a taiga woodland. *Journal of Geophysical Research: Atmospheres*, 99(D1), 1927–1936. https://doi.org/10.1029/93jd02292

Baldocchi, D. D. (2003). Assessing the eddy covariance technique for evaluating carbon dioxide exchange rates of ecosystems: past, present and future. *Global Change Biology*, 9(4), 479–492. https://doi.org/10.1046/j.1365-2486.2003.00629.x

Baldocchi, D., Falge, E., Gu, L., Olson, R., Hollinger, D., Running, S., et al. (2001). FLUXNET: A New Tool to Study the Temporal and Spatial Variability of Ecosystem–Scale Carbon Dioxide, Water Vapor, and Energy Flux Densities. *Bulletin of the American Meteorological Society*, 82(11), 2415–2434. https://doi.org/10.1175/1520-0477(2001)082<2415:fantts>2.3.co;2

Baldocchi, D. D. (2020). How eddy covariance flux measurements have contributed to our understanding of Global Change Biology. *Global Change Biology*, 26(1), 242–260. https://doi.org/10.1111/gcb.14807

Barr, A. G., Morgenstern, K., Black, T. A., McCaughey, J. H., & Nesic, Z. (2006). Surface energy balance closure by the eddy-covariance method above three boreal forest stands and implications for the measurement of the CO_2 flux. *Agricultural and Forest Meteorology*, 140(1–4), 322–337. https://doi.org/10.1016/j.agrformet.2006.08.007

Betts, A. K., & Ball, J. H. (1997). Albedo over the boreal forest. *Journal of Geophysical Research: Atmospheres*, 102(D24), 28901–28909. https://doi.org/10.1029/96jd03876

Bergeron, O., Margolis, H. A., Black, T. A., Coursolle, C., Dunn, A. L., Barr, A. G., & Wofsy, S. C. (2007). Comparison of carbon dioxide fluxes over three boreal black spruce forests in Canada. *Global Change Biology*, 13(1), 89–107. https://doi.org/10.1111/j.1365-2486.2006.01281.x

Bonan, G. B., Pollard, D., & Thompson, S. L. (1992). Effects of boreal forest vegetation on global climate. *Nature*, 359(6397), 716–718. https://doi.org/10.1038/359716a0

Bonan, G. B. (2008). Forests and Climate Change: Forcings, Feedbacks, and the Climate Benefits of Forests. *Science*, 320(5882), 1444–1449. https://doi.org/10.1126/science.1155121

Brandt, J. P., Flannigan, M. D., Maynard, D. G., Thompson, I. D., & Volney, W. J. A. (2013). An introduction to Canada's boreal zone: ecosystem processes, health, sustainability, and environmental issues1. *Environmental Reviews*, 21(4), 207–226. https://doi.org/10.1139/er-2013-0040

Biskaborn, B. K., Smith, S. L., Noetzli, J., Matthes, H., Vieira, G., Streletskiy, D. A., et al. (2019). Permafrost is warming at a global scale. *Nature Communications*, 10(1), 264. https://doi.org/10.1038/s41467-018-08240-4

Carpino, O. A., Berg, A. A., Quinton, W. L., & Adams, J. R. (2018). Climate change and permafrost thaw-induced boreal forest loss in northwestern Canada. *Environmental Research Letters*, 13(8), 084018. https://doi.org/10.1088/1748-9326/aad74e

Chen, D., Loboda, T. V., Krylov, A., & Potapov, P. V. (2016). Mapping stand age dynamics of the Siberian larch forests from recent Landsat observations. *Remote Sensing of Environment*, 187, 320–331. https://doi.org/10.1016/j.rse.2016.10.033

Commane, R., Lindaas, J., Benmergui, J., Luus, K. A., Chang, R.

Y.-W., Daube, B. C., et al. (2017). Carbon dioxide sources from Alaska driven by increasing early winter respiration from Arctic tundra. *Proceedings of the National Academy of Sciences*, 114(21), 5361–5366. https://doi.org/10.1073/pnas.1618567114

Conard, S. G., & Ivanova, G. A. (1997). Wildfire in Russian Boreal Forests—Potential Impacts of Fire Regime Characteristics on Emissions and Global Carbon Balance Estimates. *Environmental Pollution*, 98(3), 305–313. https://doi.org/10.1016/s0269-7491(97)00140-1

Cueva-González, M., Gerard, F., Balzter, H., & Riaño, D. (2009). Analysing forest recovery after wildfire disturbance in boreal Siberia using remotely sensed vegetation indices. *Global Change Biology*, 15(3), 561–577. https://doi.org/10.1111/j.1365-2486.2008.01784.x

Curtis, P. S., & Gough, C. M. (2018). Forest aging, disturbance and the carbon cycle. *New Phytologist*, 219(4), 1188–1193. https://doi.org/10.1111/nph.15227

Dolman, A. J., Maximov, T. C., Moors, E. J., Maximov, A. P., Elbers, J. A., Kononov, A. V., et al. (2004). Net ecosystem exchange of carbon dioxide and water of far eastern Siberian Larch (*Larix cajanderii*) on permafrost. Biogeosciences, 1(2), 133–146. https://doi.org/10.5194/bg-1-133-2004

Dunn, A. L., Barford, C. C., Wofsy, S. C., Goulden, M. L., & Daube, B. C. (2007). A long-term record of carbon exchange in a boreal black spruce forest: means, responses to interannual variability, and decadal trends. *Global Change Biology*, 13(3), 577–590. Https://Doi.Org/10.1111/J.1365-2486.2006.01221.X

Esper, J., & Schweingruber, F. H. (2004). Large-scale treeline changes recorded in Siberia. *Geophysical Research Letters*, 31(6), L06202. https://doi.org/10.1029/2003gl019178

Falge, E., Baldocchi, D., Olson, R., Anthoni, P., Aubinet, M., Bernhofer, C., et al. (2001). Gap filling strategies for long term energy flux data sets. *Agricultural and Forest Meteorology*, 107(1), 71–77. https://doi.org/10.1016/s0168-1923(00)00235-5

Fan, S.-M., Goulden, M. L., Munger, J. W., Daube, B. C., Bakwin, P. S., Wofsy, S. C., et al. (1995). Environmental controls on the photosynthesis and respiration of a boreal lichen woodland: a growing season of whole-ecosystem exchange measurements by eddy correlation. *Oecologia*, 102(4), 443–452. https://doi.org/10.1007/bf00341356

Fisher, J. B., Tu, K. P., & Baldocchi, D. D. (2008). Global estimates of the land–atmosphere water flux based on monthly AVHRR and ISLSCP-II data, validated at 16 FLUXNET sites. *Remote Sensing of Environment*, 112(3), 901–919. https://doi.org/10.1016/j.rse.2007.06.025

Forkel, M., Carvalhais, N., Rödenbeck, C., Keeling, R., Heimann, M., Thonicke, K., et al. (2016). Enhanced seasonal CO_2 exchange caused by amplified plant productivity in northern ecosystems. *Science*, 351(6274), 696–699. https://doi.org/10.1126/science.aac4971

Fyllas, N. M., Bentley, L. P., Shenkin, A., Asner, G. P., Atkin, O. K., Díaz, S., et al. (2017). Solar radiation and functional traits explain the decline of forest primary productivity along a tropical elevation gradient. *Ecology Letters*, 20(6), 730–740. https://doi.org/10.1111/ele.12771

Gauthier, S., Bernier, P., Kuuluvainen, T., Shvidenko, A. Z., & Schepaschenko, D. G. (2015). Boreal forest health and global change. *Science*, 349(6250), 819–822. https://doi.org/10.1126/science.aaa9092

Goldammer, J. G., & Furyaev, V. V. (1996). Fire in Ecosystems of Boreal Eurasia. *Forestry Sciences*, 1–20. https://doi.org/10.1007/978-94-015-8737-2_1

Goulden, M. L., Wofsy, S. C., Harden, J. W., Trumbore, S. E., Crill, P. M., Gower, S. T., et al. (1998). Sensitivity of Boreal Forest Carbon Balance to Soil Thaw. *Science*, 279(5348), 214–217. https://doi.org/10.1126/science.279.5348.214

Gower, S. T., & Richards, J. H. (1990). Larches: Deciduous Conifers in an Evergreen World. *BioScience*, 40(11), 818–826. https://doi.org/10.2307/1311484

Gower, S. T., Vogel, J. G., Norman, J. M., Kucharik, C. J., Steele, S. J., & Stow, T. K. (1997). Carbon distribution and aboveground net primary production in aspen, jack pine, and black spruce stands in Saskatchewan and Manitoba, Canada. *Journal of Geophysical Research: Atmospheres*, 102(D24), 29029–29041. https://doi.org/10.1029/97jd02317

Gower, S. T., Krankina, O., Olson, R. J., Apps, M., Linder, S., & Wang, C. (2001). Net primary production and carbon allocation patterns of boreal forest ecosystems. *Ecological Applications*, 11(5), 1395–1411. https://doi.org/10.1890/1051-0761(2001)011[1395:nppaca]2.0.co;2

Guo, W., Liu, H., Anenkhonov, O. A., Shangguan, H., Sandanov, D. V., Korolyuk, A. Yu., et al. (2018). Vegetation can strongly regulate permafrost degradation at its southern edge through changing surface freeze-thaw processes. *Agricultural and Forest Meteorology*, 252, 10–17. https://doi.org/10.1016/j.agrformet.2018.01.010

Hart, S. J., Henkelman, J., McLoughlin, P. D., Nielsen, S. E., Truchon-Savard, A., & Johnstone, J. F. (2019). Examining forest resilience to changing fire frequency in a fire-prone region of boreal forest. *Global Change Biology*, 25(3), 869–884. https://doi.org/10.1111/gcb.14550

Helbig, M., Chasmer, L. E., Desai, A. R., Kljun, N., Quinton, W. L., & Sonnentag, O. (2017). Direct and indirect climate change effects on carbon dioxide fluxes in a thawing boreal forest–wetland landscape. *Global Change Biology*, 23(8), 3231–3248. https://doi.org/10.1111/gcb.13638

Hermle, S., Lavigne, M. B., Bernier, P. Y., Bergeron, O., & Paré, D. (2010). Component respiration, ecosystem respiration and net primary production of a mature black spruce forest in northern Quebec. *Tree Physiology*, 30(4), 527–540. https://doi.org/10.1093/treephys/tpq002

Hollinger, D. Y., Kelliher, F. M., Schulze, E.-D., Bauer, G., Arneth, A., Byers, J. N., et al. (1998). Forest–atmosphere carbon dioxide exchange in eastern Siberia. *Agricultural and Forest Meteorology*, 90(4), 291–306. https://doi.org/10.1016/s0168-1923(98)00057-4

Ichii, K., Ueyama, M., Kondo, M., Saigusa, N., Kim, J., Alberto, Ma. C., et al. (2017). New data-driven estimation of terrestrial CO_2 fluxes in Asia using a standardized database of eddy covariance measurements, remote sensing data, and support vector regression. *Journal of Geophysical Research: Biogeosciences*, 122(4), 767–795. https://doi.org/10.1002/2016jg003640

Ikonen, J., Vehviläinen, J., Rautiainen, K., Smolander, T., Lemmetyinen, J., Bircher, S., & Pulliainen, J. (2016). The Sodankylä in situ soil moisture observation network: an example application of ESA CCI soil moisture product evaluation. *Geoscientific Instrumentation, Methods and Data Systems*, 5(1), 95–108. https://doi.org/10.5194/gi-5-95-2016

Jarvis, P. G., Massheder, J. M., Hale, S. E., Moncrieff, J. B., Rayment, M., & Scott, S. L. (1997). Seasonal variation of carbon dioxide, water vapor, and energy exchanges of a boreal black spruce forest. *Journal of Geophysical Research: Atmospheres*, 102(D24), 28953–28966. https://doi.org/10.1029/97jd01176

Joiner, J., Yoshida, Y., Vasilkov, A. P., Schaefer, K., Jung, M., Guanter, L., et al. (2014). The seasonal cycle of satellite chlorophyll fluorescence observations and its relationship to vegetation phenology and ecosystem atmosphere carbon exchange. *Remote Sensing of Environment*, 152, 375–391. https://doi.org/10.1016/j.rse.2014.06.022

Kljun, N., Calanca, P., Rotach, M. W., & Schmid, H. P. (2004). A Simple Parameterisation for Flux Footprint Predictions. *Boundary-Layer Meteorology*, 112(3), 503–523. https://doi.org/10.1023/b:boun.0000030653.71031.96

Kolari, P., Pumpanen, J., Rannik, Ü., Ilvesniemi, H., Hari, P., & Berninger, F. (2004). Carbon balance of different aged Scots pine forests in Southern Finland. *Global Change Biology*, 10(7), 1106–1119. https://doi.org/10.1111/j.1529-8817.2003.00797.x

Kurbatova, J., Li, C., Varlagin, A., Xiao, X., & Vygodskaya, N. (2008). Modeling carbon dynamics in two adjacent spruce forests with different soil conditions in Russia. *Biogeosciences*, 5(4), 969–980. https://doi.org/10.5194/bg-5-969-2008

Kwon, M. J., Heimann, M., Kolle, O., Luus, K. A., Schuur, E. A. G., Zimov, N., et al. (2016). Long-term drainage reduces CO_2 uptake and increases CO_2 emission on a Siberian floodplain due to shifts in vegetation community and soil thermal characteristics. *Biogeosciences*, 13(14), 4219–4235. https://doi.org/10.5194/bg-13-4219-2016

Litvak M, Miller S, Wofsy S C and Goulden M 2003 Effect of stand age on whole ecosystem CO_2 exchange in the Canadian boreal forest *J. Geophys. Res. Atmos.* 108(D3) 8225

Liu, H., & Randerson, J. T. (2008). Interannual variability of surface energy exchange depends on stand age in a boreal forest fire chronosequence. Journal of Geophysical Research: Biogeosciences (2005–2012), 113(G1), G01006. https://doi.org/10.1029/2007jg000483

Liu, J., Cheng, F., Munger, W., Jiang, P., Whitby, T. G., Chen, S., et al. (2020). Precipitation extremes influence patterns and partitioning of evapotranspiration and transpiration in a deciduous boreal larch forest. *Agricultural and Forest Meteorology*, 287, 107936. https://doi.org/10.1016/j.agrformet.2020.107936

Liu, Z., Kimball, J. S., Parazoo, N. C., Ballantyne, A. P., Wang, W. J., Madani, N., et al. (2019). Increased high-latitude photosynthetic carbon gain offset by respiration carbon loss during an anomalous warm winter to spring transition. *Global Change Biology*, 26(2), 682–696. https://doi.org/10.1111/gcb.14863

Luo, Z., Feng, W., Luo, Y., Baldock, J., & Wang, E. (2017). Soil organic carbon dynamics jointly controlled by climate, carbon inputs, soil properties and soil carbon fractions. *Global Change Biology*, 23(10), 4430–4439. https://doi.org/10.1111/gcb.13767

Luus, K. A., & Lin, J. C. (2015). The Polar Vegetation Photosynthesis and Respiration Model: a parsimonious, satellite-data-driven model of high-latitude CO_2 exchange. *Geoscientific Model Development*, 8(8), 2655–2674. https://doi.org/10.5194/gmd-8-2655-2015

Luus, K. A., Commane, R., Parazoo, N. C., Benmergui, J., Euskirchen, E. S., Frankenberg, C., et al. (2017). Tundra photosynthesis captured by satellite-observed solar-induced chlorophyll fluorescence. *Geophysical Research Letters*, 44(3), 1564–1573. https://doi.org/10.1002/2016gl070842

Mack, M. C., Treseder, K. K., Manies, K. L., Harden, J. W., Schuur, E. A. G., Vogel, J. G., et al. (2008). Recovery of Aboveground Plant Biomass and Productivity After Fire in Mesic and Dry Black Spruce Forests of Interior Alaska. *Ecosystems*, 11(2), 209–225. https://doi.org/10.1007/s10021-007-9117-9

Mahadevan, P., Wofsy, S. C., Matross, D. M., Xiao, X., Dunn, A. L., Lin, J. C., et al. (2008). A satellite-based biosphere parameterization for net ecosystem CO2 exchange: Vegetation Photosynthesis and Respiration Model (VPRM). *Global Biogeochemical Cycles*, 22(2), n/a-n/a. https://doi.org/10.1029/2006gb002735

Mäki M, Krasnov D, Hellén H, Noe S M and Bäck J 2019 Mäki, M., Krasnov, D., Hellén, H., Noe, S. M., & Bäck, J. (2019). Stand type affects fluxes of volatile organic compounds from the forest floor in hemiboreal and boreal climates. *Plant and Soil*, 441(1–2), 363–381. https://doi.org/10.1007/s11104-019-04129-3

Matsumoto, K., Ohta, T., Nakai, T., Kuwada, T., Daikoku, K., Iida, S., et al. (2008). Energy consumption and evapotranspiration at several boreal and temperate forests in the Far East. *Agricultural and Forest Meteorology*, 148(12), 1978–1989. https://doi.org/10.1016/j.agrformet.2008.09.008

Medvigy, D., Wofsy, S. C., Munger, J. W., Hollinger, D. Y., & Moorcroft, P. R. (2009). Mechanistic scaling of ecosystem function and dynamics in space and time: Ecosystem Demography model version 2. *Journal of Geophysical Research: Biogeosciences* (2005–2012), 114(G1). https://doi.org/10.1029/2008jg000812

Meyer, N., Welp, G., & Amelung, W. (2018). The temperature sensitivity (Q_{10}) of soil respiration: controlling factors and spatial prediction at regional scale based on environmental soil classes. *Global Biogeochemical Cycles*, 32(2), 306–323. https://doi.org/10.1002/2017gb005644

Miles, V. V., & Esau, I. (2016). Spatial heterogeneity of greening and browning between and within bioclimatic zones in northern West Siberia. *Environmental Research Letters*, 11(11), 115002. https://doi.org/10.1088/1748-9326/11/11/115002

Milyukova, I. M., Kolle, O., Varlagin, A. V., Vygodskaya, N. N., Schulze, E. D., & Lloyd, J. (2016). Carbon balance of a southern taiga spruce stand in European Russia. *Tellus B*, 54(5), 429–442. https://doi.org/10.3402/tellusb.v54i5.16679

Nakai, Y., Matsuura, Y., Kajimoto, T., Abaimov, A. P., Yamamoto, S., & Zyryanova, O. A. (2008). Eddy covariance CO_2 flux above a *Gmelin larch* forest on continuous permafrost in Central Siberia during a growing season. *Theoretical and Applied Climatology*, 93(3–4), 133–147. https://doi.org/10.1007/s00704-007-0337-x

Natali, S. M., Watts, J. D., Rogers, B. M., Potter, S., Ludwig, S. M., Selbmann, A. K., et al. (2019). Large loss of CO2 in winter observed across the northern permafrost region. *Nature Climate Change*, 9(11), 852–857. https://doi.org/10.1038/s41558-019-0592-8

Nolan, C., Overpeck, J. T., Allen, J. R. M., Anderson, P. M., Betancourt, J. L., Binney, H. A., et al. (2018). Past and future global transformation of terrestrial ecosystems under climate change. *Science*, 361(6405), 920–923. https://doi.org/10.1126/science.aan5360

Odum, E. P. (1969). The Strategy of Ecosystem Development. *Science*, 164(3877), 262–270. https://doi.org/10.1126/science.164.3877.262

Ohta, T., Kotani, A., Iijima, Y., Maximov, T. C., Ito, S., Hanamura, M., et al. (2014). Effects of waterlogging on water and carbon dioxide fluxes and environmental variables in a Siberian larch forest, 1998–2011. *Agricultural and Forest Meteorology*, 188, 64–75. https://doi.org/10.1016/j.agrformet.2013.12.012

Outcalt, S. I., Nelson, F. E., & Hinkel, K. M. (1990). The zero-curtain effect: Heat and mass transfer across an isothermal region in freezing soil. *Water Resources Research*, 26(7), 1509–1516. https://doi.org/10.1029/wr026i007p01509

Pan, Y., Birdsey, R. A., Fang, J., Houghton, R., Kauppi, P. E., Kurz, W. A., et al. (2011). A Large and Persistent Carbon Sink in the World's Forests. *Science*, 333(6045), 988–993. https://doi.org/10.1126/science.1201609

Papale, D., Reichstein, M., Aubinet, M., Canfora, E., Bernhofer, C., Kutsch, W., et al. (2006). Towards a standardized processing of Net Ecosystem Exchange measured with eddy covariance technique: algorithms and uncertainty estimation. *Biogeosciences*, 3(4), 571–583. https://doi.org/10.5194/bg-3-571-2006

Pattey, E., Desjardins, R. L., & St-Amour, G. (1997). Mass and energy exchanges over a black spruce forest during key periods of BOREAS 1994. *Journal of Geophysical Research: Atmospheres*, 102(D24), 28967–28975. https://doi.org/10.1029/97jd01329

Peng, C., Ma, Z., Lei, X., Zhu, Q., Chen, H., Wang, W., et al. (2011). A drought-induced pervasive increase in tree mortality across Canada's boreal forests. *Nature Climate Change*, 1(9), 467–471. https://doi.org/10.1038/nclimate1293

Fei, P., Manhou, X., Quangang, Y., Xuhui, Z., Tao, W., & Xian, X. (2015). Different Responses of Soil Respiration and Its Components to Experimental Warming with Contrasting Soil Water Content. *Arctic, Antarctic, and Alpine Research*, 47(2), 359–368. https://doi.org/10.1657/aaar0014-018

Pries, C. E. H., Schuur, E. A. G., & Crummer, K. G. (2013). Thawing permafrost increases old soil and autotrophic respiration in tundra: Partitioning ecosystem respiration using 13C and 14C. *Global Change Biology*, 19(2), 649–661. https://doi.org/10.1111/gcb.12058

Quan, X., & Wang, C. (2018). Acclimation and adaptation of leaf photosynthesis, respiration and phenology to climate change: A 30-year *Larix gmelinii* common-garden experiment. *Forest Ecology and Management*, 411, 166–175. https://doi.org/10.1016/j.foreco.2018.01.024

Reichstein, M., Falge, E., Baldocchi, D., Papale, D., Aubinet, M., Berbigier, P., et al. (2005). On the separation of net ecosystem exchange into assimilation and ecosystem respiration: review and improved algorithm. *Global Change Biology*, 11(9), 1424–1439. https://doi.org/10.1111/j.1365-2486.2005.001002.x

Reim, A., Lüke, C., Krause, S., Pratscher, J., & Frenzel, P. (2012). One millimetre makes the difference: high-resolution analysis of methane-oxidizing bacteria and their specific activity at the oxic–anoxic interface in a flooded paddy soil. The ISME Journal, 6(11), 2128–2139. https://doi.org/10.1038/ismej.2012.57

Sala, O. E., Chapin, F. S., III, Armesto, J. J., Berlow, E., Bloomfield, J., et al. (2000). Global Biodiversity Scenarios for the Year 2100. *Science*, 287(5459), 1770–1774. https://doi.org/10.1126/science.287.5459.1770

Luyssaert, S., Schulze, E.-D., Börner, A., Knohl, A., Hessenmöller, D., Law, B. E., et al. (2008). Old-growth forests as global carbon sinks. *Nature*, 455(7210), 213–215. https://doi.org/10.1038/nature07276

Schuur, E. A. G., Vogel, J. G., Crummer, K. G., Lee, H., Sickman, J. O., & Osterkamp, T. E. (2009). The effect of permafrost thaw on old carbon release and net carbon exchange from tundra. *Nature*, 459(7246), 556–559. https://doi.org/10.1038/nature08031

Shen, M., Tang, Y., Desai, A. R., Gough, C., & Chen, J. (2014). Can EVI-derived land-surface phenology be used as a surrogate for phenology of canopy photosynthesis? *International Journal of Remote Sensing*, 35(3), 1162–1174. https://doi.org/10.1080/01431161.2013.875636

Shuman, J. K., Shugart, H. H., & O'halloran, T. L. (2011). Sensitivity of Siberian larch forests to climate change. *Global Change Biology*, 17(7), 2370–2384. https://doi.org/10.1111/j.1365-2486.2011.02417.x

Sutinen, M.-L., Palta, J. P., & Reich, P. B. (1992). Seasonal differences in freezing stress resistance of needles of Pinus nigra and *Pinus resinosa*: evaluation of the electrolyte leakage method. *Tree Physiology*, 11(3), 241–254. https://doi.org/10.1093/treephys/11.3.241

Sulla-Menashe, D., Woodcock, C. E., & Friedl, M. A. (2018). Canadian boreal forest greening and browning trends: an analysis of biogeographic patterns and the relative roles of disturbance versus climate drivers. *Environmental Research Letters*, 13(1), 014007. https://doi.org/10.1088/1748-9326/aa9b88

Takata, K., Patra, P. K., Kotani, A., Mori, J., Belikov, D., Ichii, K., et al. (2017). Reconciliation of top-down and bottom-up CO2 fluxes in Siberian larch forest. *Environmental Research Letters*, 12(12), 125012. https://doi.org/10.1088/1748-9326/aa926d

Turner, D. P., Ritts, W. D., Cohen, W. B., Gower, S. T., Running, S. W., Zhao, M., et al. (2006). Evaluation of MODIS NPP and GPP products across multiple biomes. *Remote Sensing of Environment*, 102(3–4), 282–292. https://doi.org/10.1016/j.rse.2006.02.017

Thum, T., Aalto, T., Laurila, T., Aurela, M., Lindroth, A., & Vesala, T. (2008). Assessing seasonality of biochemical CO2 exchange model parameters from micrometeorological flux observations at boreal coniferous forest. *Biogeosciences*, 5(6), 1625–1639. https://doi.org/10.5194/bg-5-1625-2008

Ueyama, M., Iwata, H., Harazono, Y., Euskirchen, E. S., Oechel, W. C., & Zona, D. (2013). Growing season and spatial variations of carbon fluxes of Arctic and boreal ecosystems in Alaska (USA). Ecological Applications, 23(8), 1798–1816. https://doi.org/10.1890/11-0875.1

Villarreal, S., Guevara, M., Alcaraz-Segura, D., Brunsell, N. A., Hayes, D., Loescher, H. W., & Vargas, R. (2018). Ecosystem functional diversity and the representativeness of environmental networks across the conterminous United States. Agricultural and Forest Meteorology, 262, 423–433. https://doi.org/10.1016/j.agrformet.2018.07.016

Wang, H., Saigusa, N., Zu, Y., Wang, W., Yamamoto, S., & Kondo, H. (2008). Carbon fluxes and their response to environmental variables in a Dahurian larch forest ecosystem in northeast China. *Journal of Forestry Research*, **19**(1), 1–10. https://doi.org/10.1007/s11676-008-0001-z

Wang, C., Han, Y., Chen, J., Wang, X., Zhang, Q., & Bond-Lamberty, B. (2013). Seasonality of soil CO2 efflux in a temperate forest: Biophysical effects of snowpack and spring freeze–thaw cycles. *Agricultural and Forest Meteorology*, 177, 83–92. https://doi.org/10.1016/j.agrformet.2013.04.008

Wang, W., Xu, J., Gao, Y., Bogoev, I., Cui, J., Deng, L., et al. (2016). Performance Evaluation of an Integrated Open-Path Eddy Covariance System in a Cold Desert Environment. *Journal of Atmospheric and Oceanic Technology*, 33(11), 2385–2399. https://doi.org/10.1175/jtech-d-15-0149.1

Walther, S., Voigt, M., Thum, T., Gonsamo, A., Zhang, Y., Köhler, P., et al. (2016). Satellite chlorophyll fluorescence measurements reveal large-scale decoupling of photosynthesis and greenness dynamics in boreal evergreen forests. *Global Change Biology*, 22(9), 2979–2996. https://doi.org/10.1111/gcb.13200

Watson, J. E. M., Venter, O., Lee, J., Jones, K. R., Robinson, J. G., Possingham, H. P., & Allan, J. R. (2018). Protect the last of the wild. *Nature*, 563(7729), 27–30. https://doi.org/10.1038/d41586-018-07183-6

Way, D. A., Crawley, C., & Sage, R. F. (2013). A hot and dry future: warming effects on boreal tree drought tolerance. *Tree Physiology*, 33(10), 1003–1005. https://doi.org/10.1093/treephys/tpt092

Zhang, J.-H., Han, S.-J., & Yu, G.-R. (2006). Seasonal variation in carbon dioxide exchange over a 200-year-old Chinese broad-leaved Korean pine mixed forest. *Agricultural and Forest Meteorology*, 137(3–4), 150–165. https://doi.org/10.1016/j.agrformet.2006.02.004

Zhang, N., Yasunari, T., & Ohta, T. (2011). Dynamics of the larch taiga–permafrost coupled system in Siberia under climate change. *Environmental Research Letters*, 6(2), 024003. https://doi.org/10.1088/1748-9326/6/2/024003

Zona, D., Gioli, B., Commane, R., Lindaas, J., Wofsy, S. C., Miller, C. E., et al. (2016). Cold season emissions dominate the Arctic tundra methane budget. *Proceedings of the National Academy of Sciences*, 113(1), 40–45. https://doi.org/10.1073/pnas.1516017113